NASA Technical Memorandum 86235

Intraplate Deformation Due To Continental Collisions: A Numerical Study of Deformation In A Thin Viscous Sheet

Steven C. Cohen
Richard C. Morgan

October 1985

NASA

NASA Technical Memorandum 86235

/ NC 999967

Intraplate Deformation Due To Continental Collisions: A Numerical Study of Deformation In A Thin Viscous Sheet

Steven C. Cohen
Richard C. Morgan
Geodynamics Branch
Goddard Space Flight Center
Greenbelt, Maryland

NASA

National Aeronautics and
Space Administration

Goddard Space Flight Center
Greenbelt, Maryland 20771

INTRODUCTION

The collision of tectonic plates involving large continental masses can produce significant crustal deformations, not only in the vicinity of the plate boundary, but also well into the interior of the plates. The best studied example of a contemporary continental collision is that involving the Indian and Eurasian plates, but other examples of both contemporary and ancient collisions are well known. The former category includes the collision between the Arabian and Eurasian Plates resulting in deformation in the Zagros Crush Zone, Anatolia, and elsewhere, and the incipient collision between Africa and the European portion of Eurasia. Ancient orogenic zones which display residual evidence of past continental collision include the Appalachian-Caledonian system, the Hercynian System in central Europe, and the Urals (Condie, 1982). Despite the attention given to both the general phenomena involved in continental collisions and to the geotectonics of specific collisions, the mechanical processes are still not well understood. In fact, controversy still exists about the correct kinematic description of the Indian-Eurasian collision. Nevertheless, the recent progress that has been made in understanding continental tectonics has sparked the emergence of several prototype models of collisional processes. The first of these models is the continental analog of the subduction of oceanic lithosphere under a continental plate near an oceanic trench. In the continental collision case crust from one plate overrides that of the other. The partial subduction of crust from one of the plates (which may have had a significant oceanic component as in the case of the Indian Plate) may be at a shallow angle with the possibility of considerable horizontal motion, or at a steep angle with implied penetration of the lithospheric plate into the mantle. In the case of the Indian-Eurasian colli-sion, there is little doubt that overthrusting of Asian continental crust onto lithospheric material from the oceanic portion of Indian plate occurred during the closing of the Tethys ocean. While localized thrusting occurs today in the vicinity of the Himalayas, it seems unlikely that this model can be used in the Tibet region, north of the Indus suture. One difficulty with the model is the fact that the buoyant Indian crust would tend to resist subduction. Both the absence of northly directed compres-

1

sional seismic activity, and the general absence of intermediate and deep depth seismic activity around Tibet argue against using this model to explain deformation within the Eurasian plate.

A second model assumes a viscous deformation of one plate as a consequence of the ram-like penetration into this plate by a more rigid collisional partner. This model is not suitable for studying the thrusting responsible for the Himalaya orogen, but it has been used with considerable success by Tapponier and Molnar (1977) and others to explain the eastward extrusion of Tibet along the Altyn Tagh and Kun-Lun faults, the plateau-like thickening of Tibetan crust, and a number of other Asiatic tectonic features.

A third model involving the shearing of thin layers of crust and their overthrusting one on top of another to accommodate the convergence between the plates has come to be known as "flake tectonics" (Oxburgh, 1972) and has been used in the study of both Appalachian and Alpian geological features.

A model for Tibet in which the uniform topography is explained by having the plateau float like a hydrostatic head on a fluid has been discussed by several authors. Recently Zhao and Morgan (1985) expressed the view that relatively cold and rigid Indian crust is penetrating into warm, low viscosity Asiatic lower crust with Tibet rising in response to the induced hydrostatic pressure. These various models are not entirely mutually exclusive and many variants of each model can be advanced.

In this paper we propose to explore in some depth various features of the punch/viscous sheet model of continental deformation. Our aim here is to understand the details of the model and to test how sensitive the model predictions are to the choices of numerical values for the parameters and to some of the implicit and explicit assumptions. We will limit the analysis to cases having simple geometries where our intuitive insight is sharper than might be the case for geologically truer condi-

tions. We refer the interested reader to the papers in the references for more detailed discussions of the model justifications and its applicability to specific contemporary environments.

MODEL DESCRIPTION

Figure 1 shows one version of the punch/deformable sheet model. By and large we will employ the mathematical development of this model that was derived by England and McKenzie (1982, 1983). Original calculations based on this model used finite difference techniques which required that the punch boundary condition be expressed as a flux of material rather than a rigid indentation. Houseman and England (1985) improved the model by using finite element techniques with prescribed boundary velocity conditions representing the punch motion. We use our own formulation of the
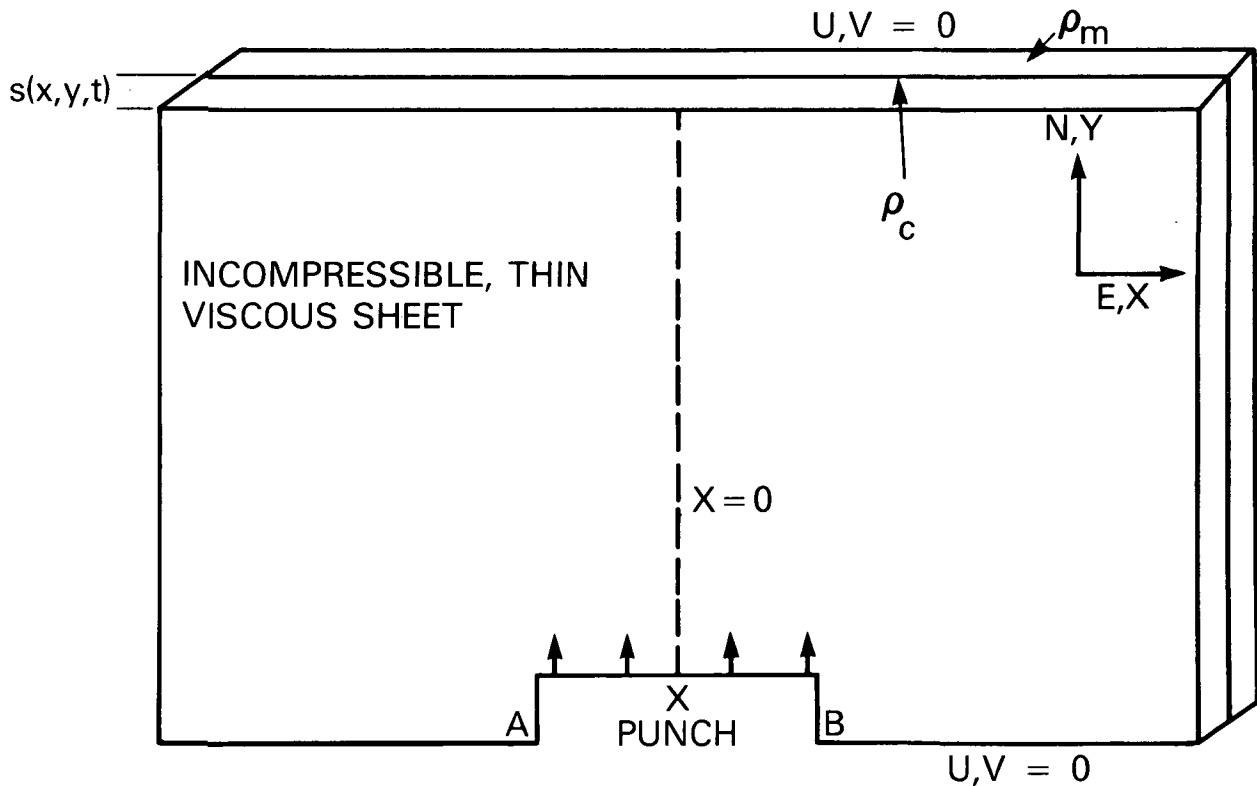

Figure 1: Punch/viscous sheet model of continental collisions. The penetration of a rigid punch into a deformable sheet is represented by moving the boundary between points A and B northward at a uniform, constant velocity. Stress and deformation variables are averaged over the depth of the sheet. The sheet has a two layer density structure. The crustal density is ϱ_c; this layer has a thickness, s. The mantle density is ϱ_m. The sheet is thin compared to its length and breadth, is subject to gravitational as well as collisional stresses, and deforms as an incompressible viscous fluid.

3

finite element approach with differences from the earlier work that will be introduced in the discussions to follow. The viscous sheet is assumed to be incompressible and in local isostatic equilibrium. The isostacy condition is maintained by Airy type compensation against a crustless ocean plate. The sheet thickness is assumed to be small compared to its length (the X or eastward direction) and breadth (the Y or northward direction).

The deformation of the sheet is governed by a power law flow of the form:

$$\tau_{ij} = B\dot{E}^{(\frac{1}{n}-1)} \dot{\varepsilon}_{ij} \tag{1}$$

where τ_{ij} and $\dot{\varepsilon}_{ij}$ are components of the deviatoric stress and the strain rate tensor respectively, $\dot{E}$ is the second invariant of the strain rate tensor, and n is a power coefficient for linear (n=1) or nonlinear (n>1) flow. The stress and strain rate variables are averaged over the thickness of the plate. The density structure of the plate is two layered. The crust has a density ϱ_c and a thickness, s (initial value s_0); the underlying mantle has a density ϱ_m. The initial thickness of the sheet is L; after collision its thickness at a point x,y is L+h(x,y) where h can be interpreted as a topographic height and we require h<<L everywhere. The isostatic condition relates the crustal thickness, topographic height, and densities:

$$h = s(1 - \varrho_c/\varrho_m) \tag{2}$$

The depth averaged equilibrium equations provide the quasi-static equations of motion for the model (England and McKenzie; 1982, 1983), viz,

$$\frac{\partial}{\partial x}\left[B\dot{E}^{(\frac{1}{n}-1)}\left(2\frac{\partial u}{\partial x} + \frac{\partial v}{\partial y}\right)\right] + \frac{\partial}{\partial y}\left[B\dot{E}^{(\frac{1}{n}-1)}\frac{1}{2}\left(\frac{\partial u}{\partial y} + \frac{\partial v}{\partial x}\right)\right]$$
$$= \frac{g\,\varrho_c}{2L}(1 - \varrho_c/\varrho_m)\frac{\partial s^2}{\partial x} \tag{3}$$

4

and

$$\frac{\partial}{\partial y}\left[B\dot{E}^{(\frac{1}{n}-1)}\left(2\frac{\partial v}{\partial y} + \frac{\partial u}{\partial x}\right)\right] + \frac{\partial}{\partial x}\left[B\dot{E}^{(\frac{1}{n}-1)}\frac{1}{2}\left(\frac{\partial u}{\partial y} + \frac{\partial v}{\partial x}\right)\right]$$

$$= \frac{g\ \varrho_c}{2L}\ (1 - \varrho_c/\varrho_m)\ \frac{\partial s^2}{\partial y} \tag{4}$$

where u and v are the velocities in the x and y directions respectively. The left hand sides of Equations 3 and 4 contain dynamical quantities relating to the velocity field; while the right hand sides contain thickness and density variables which are quantities related to the gravitational stresses. The equilibrium conditions can be solved for the velocity field whenever the crustal thicknesses are known. In the general case, the continuity or conservation of mass condition provides a third equation for the three unknown quantities: u(x,y,t), v(x,y,t), and s(x,y,t). For finite difference calculations the continuity condition is best expressed in an Eulerian frame of reference with fixed positions for all nodal points. The Eulerian frame can also be used with finite element calculations, but a Langranian frame in which nodal points move with the material flow, is more convenient. In this frame of reference the continuity condition expressing conservation of crustal mass is:

$$\frac{\partial s}{\partial t} = -s\left(\frac{\partial u}{\partial x} + \frac{\partial v}{\partial y}\right) = -s\ (\dot{\varepsilon}_{xx} + \dot{\varepsilon}_{yy}) = s\ \dot{\varepsilon}_{zz} \tag{5}$$

The last form of the equality is a consequence of the incompressiblity condition,

$$\dot{\varepsilon}_{xx} + \dot{\varepsilon}_{yy} + \dot{\varepsilon}_{zz} = 0 \tag{6}$$

As we will now show the equilibrium equations have a useful and particularly simple form for a linear rheology. First we define a term, the gravitational strain rate, $\dot{\varepsilon}_g$, which has strain rate units and can be used to express the contribution of gravity to the equilibrium conditions,

$$\dot{\varepsilon}_g = \frac{g\ \varrho_c(1 - \varrho_c/\varrho_m)\ s^2}{BL} \tag{7}$$

5

The parameter $B = 2\eta$ where η is the viscosity. The linear equilibrium equations can now be written

$$4\frac{\partial^2 u}{\partial x^2} + \frac{\partial^2 u}{\partial y^2} + 3\frac{\partial^2 v}{\partial x \partial y} = \frac{\partial}{\partial x}\left[\frac{g\ \varrho_c(1 - \varrho_c/\varrho_m)s^2}{BL}\right] \tag{8a}$$

or

$$2\frac{\partial \dot{\varepsilon}_{xx}}{\partial x} + \frac{\partial \dot{\varepsilon}_{yy}}{\partial x} + \frac{\partial \dot{\varepsilon}_{xy}}{\partial y} = \frac{1}{2}\frac{\partial \dot{\varepsilon}_g}{\partial x} \tag{8b}$$

and

$$4\frac{\partial^2 v}{\partial y^2} + \frac{\partial^2 v}{\partial x^2} + 3\frac{\partial^2 u}{\partial y \partial x} = \frac{\partial}{\partial y}\left[\frac{g\ \varrho_c(1 - \varrho_c/\varrho_m)s^2}{BL}\right] \tag{9a}$$

or

$$2\frac{\partial \dot{\varepsilon}_{yy}}{\partial y} + \frac{\partial \dot{\varepsilon}_{xx}}{\partial y} + \frac{\partial \dot{\varepsilon}_{xy}}{\partial x} = \frac{1}{2}\frac{\partial \dot{\varepsilon}_g}{\partial y} \tag{9b}$$

When the terms involving the gravitational strain are small, the equilibrium equations can be solved for the velocities; these velocities can then be used in the continuity equation. In the general case, the three equations must be solved simultaneously. Once the velocities and strain rate have been determined, deviatoric stresses can be calculated from the rheological law. To calculate total stresses, the thickness averaged pressure, P, must be known:

$$P = \frac{1}{2}[g\ \varrho_m L + B\dot{\varepsilon}_g] - (\tau_{xx} + \tau_{yy}) \tag{10}$$

Contraction is taken to be negative, extension positive, in our calculations.

The parameters that enter explicitly into the problem are the rheological constants, B (or η) and n, the lithosphere thickness, L, and the densities, ϱ_c and ϱ_m. Initial conditions are imposed on the crustal thickness at the nodes, and boundary conditions are imposed on the velocities and (if desired) the thicknesses along the grid border. Constraints can be applied on the thickness of individual mesh points. The geometry of the plate is expressed through the set of grid parameters.

RESULTS

A prototype case we have investigated involves a linear rheology with parameters chosen as in Table I. Our finite element grid consists of 361 nodes arranged in four node elements. The 324 elements are initially squares with sides 200 km in length. The original grid is 3600 km in both length and breadth. A limited number of calculations were made with finer mesh grids to verify the general results presented here. We have taken configurations in which there is symmetry about the midpoint of the punch in Figure 1. The grid represents the right hand side of the deforming sheet; i.e., X=0 is the midpoint of the punch. The punch has a uniform velocity of 50 mm/yr in a direction parallel to the y axis (northward) for values of X less than or equal to 1200 km. The bottom boundary of the sheet is held fixed for nodes at 1400 km and beyond. The top boundary is held fixed, but we have investigated the deformation for two lateral boundary conditions: one when the side boundary is held fixed and one where free slip is allowed (a stree free right hand boundary). Figure 2 shows velocity distributions at t=0+, a time immediately after initial contact between the punch and sheet. In front of the punch, material flows generally northward to escape the indentation.

Table I: Numerical Parameters Used in Finite Element Model

initial plate length: 3600 km

plate breadth: 3600 km

initial plate thickness, $L = 100$ km

initial crustal thickness, $s_0 = 35$ km

punch velocity: 50 mm/yr = 50 km/Myr northward

punch width (center to edge): 1200 km

crustal density, ϱ_c, = 2.80 gm/cm^3

mantle density, ϱ_m, = 3.30 gm/cm^3
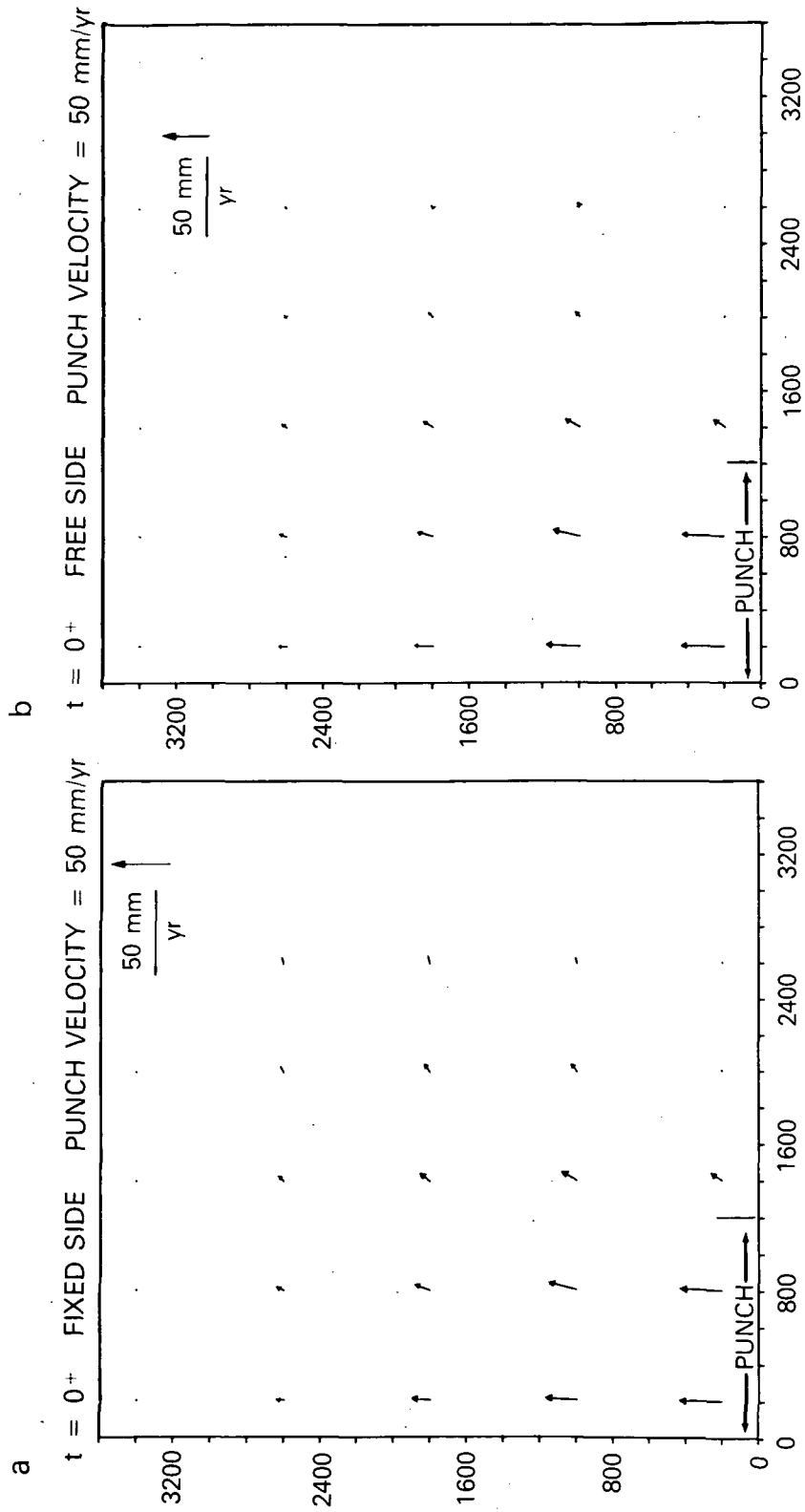
$B (=2 \eta) = 1 \times 10^{24}$ Pa. sec

7

Figure 2: a. Velocity vectors at t=0+. The initial sheet dimensions are 3600 km × 3600 km × 100 km. The punch center is at X=0, its edge at 1200 km. The side boundary is held fixed.

b. Same as "a" except the side boundary is unconstrained.

8

Further away, particularly to the northeast there is a tendency for material to flow toward the side of

the grid; again in an attempt to move away from the zone of impact compression. As the side wall

is approached the flow is outward for a free boundary, but must vanish for a fixed boundary. In the

calculations shown on Figure 2, the side boundary is sufficiently far away that the velocities appear

to vanish on the scale of the figure. However as later figures will show, the deformation at this

boundary is not negligible. To the side of the indenter, a low pressure regime will develop as the

punch progresses inward. As we will see in a moment, this becomes a region of crustal thinning and

shearing or extensional movement.

Some of the features of the collision model can be seen in more detail in Figure 3 which shows

the distorted grid and crustal thicknesses after punch penetration has advanced one-third of the way
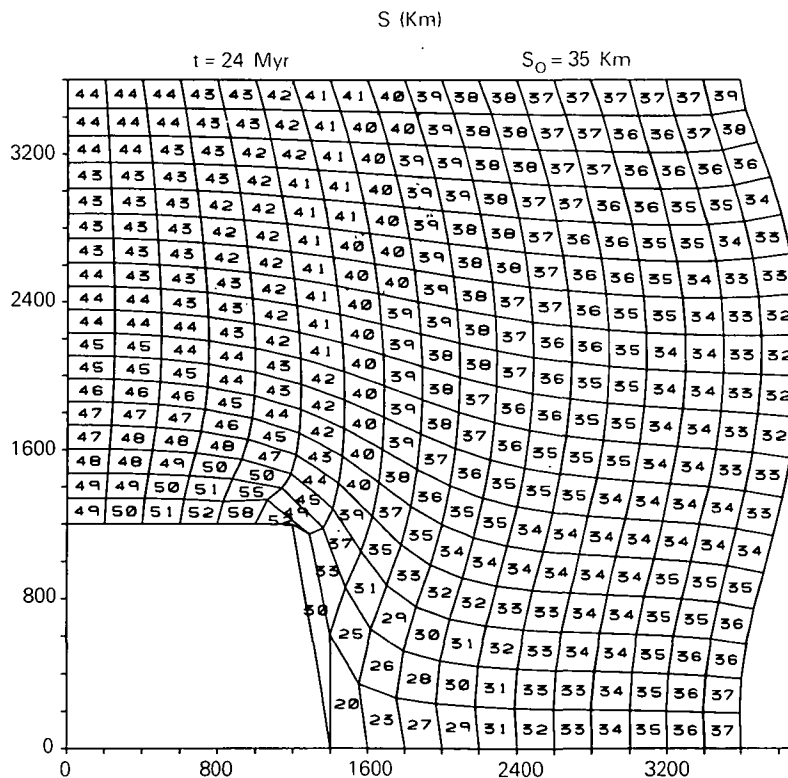

Figure 3: Grid distortions and crustal thicknesses (in km) after 24 million years. The grid elements are initially squares with sides of 200 km. The initial crustal thickness is 35 km. The right hand side is unconstrained. The element thickness values are the average of the values obtained at the four nodes of the element.

through the plate (at a velocity of 50 mm/yr, a distance of 1200 km is covered in 24 million years). The thickening of the crust is concentrated near the corner of the punch (but not at the edge due, in part, to the discrete nature of the finite element grid). The intense deformation in front of the corner of the punch is manifest by the distortion of the grid elements near that locale. Crustal thicknesses near the center of the punch are still substantial but not as large as those near the corner. As distance from the punch increases, there is a much more rapid decrease in crustal thickness for points located in front of the punch corner than for those in front of the punch center. To the side of the punch, the aforementioned low pressure zone manifests itself in the dilatation of the elements and the thinning of the crust. The bowing of the (free slip) right hand boundary results in crustal thinning in the boundary midsection and thickening toward the ends. Figure 3 should be compared to Figure 4 which shows the results when the lateral boundary is fixed. In general, crustal thicknesses are greater in the latter because material cannot expand beyond the original sides. In front of the
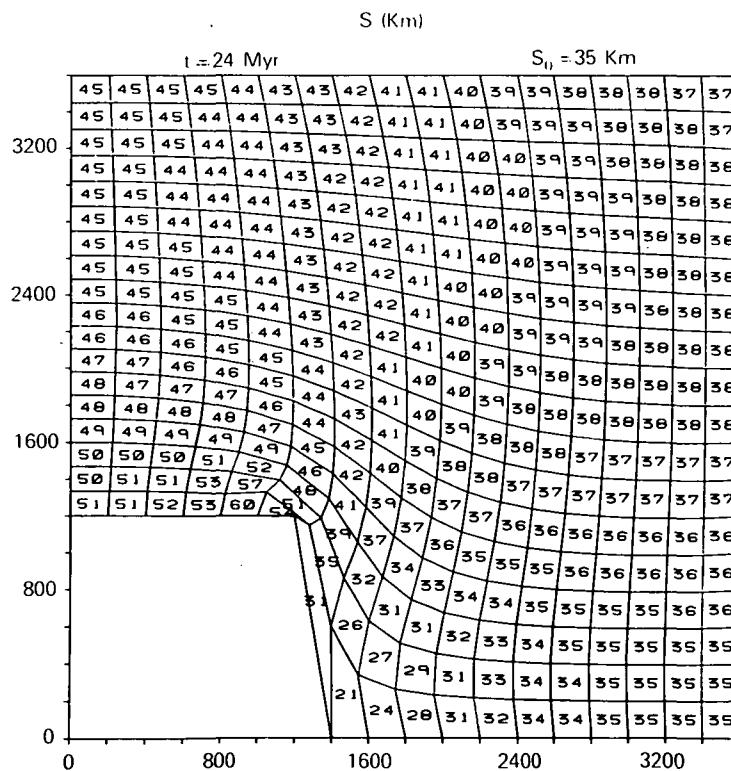
Figure 4: Same as Figure 3 except the right hand side is fixed.

punch, the qualitative features are very similar in the two cases. Therefore, when the aspect ratio of the punch diameter to sheet length is one-third or greater it appears that the deformation in front of the punch is controlled by the punch and not the lateral boundary conditions. Proceeding to the side, the differences between the two models become more pronounced as boundary effects become dominant. We have verified these conclusions by performing simulations with both smaller and larger punches. When the punch diameter exceeds fifty percent of the sheet length, the effects of the indentation are ubiquitous.

The calculations shown in Figures 3 and 4 were terminated at 24 million years because the elements near the punch corner had become quite distorted. If the calculations were extended for a greater period, numerical instabilities would be introduced. We note, however, that the calculations could be extended in time by redefining the finite element grid and transforming all variables onto the new grid. Since the punch has already penetrated one-third of the way into the sheet by 24 million years we chose not to introduce this complexity into our calculations. The choice of 24 million years is arbitrary. By choosing larger distances between the nodal points, but maintaining all other parameters the integration could be extended further in time, but with some loss of spatial resolution. Spatial resolution could be improved by using a finer grid, but the calculations would require greater computer time and storage. The calculations can also be extended in time by using a less abrupt edge for the punch as in Houseman and England (1985). However this alters the deformation pattern (see discussion below).

Figures 5 and 6 focus attention on the instantaneous crustal thickening rates rather than the integrated thickness over time. At $t = 0+$, the crustal thickening rates (which are shown as element values obtained by computing the mean of the four nodal values) have maximum values on the order of 1 mm/yr for the cases illustrated. The maximum rates are concentrated near the punch corner. After 24 million years the situation has changed somewhat. The region with moderate to large crustal thickening rates has grown larger and the location of the maximum has moved in front of the
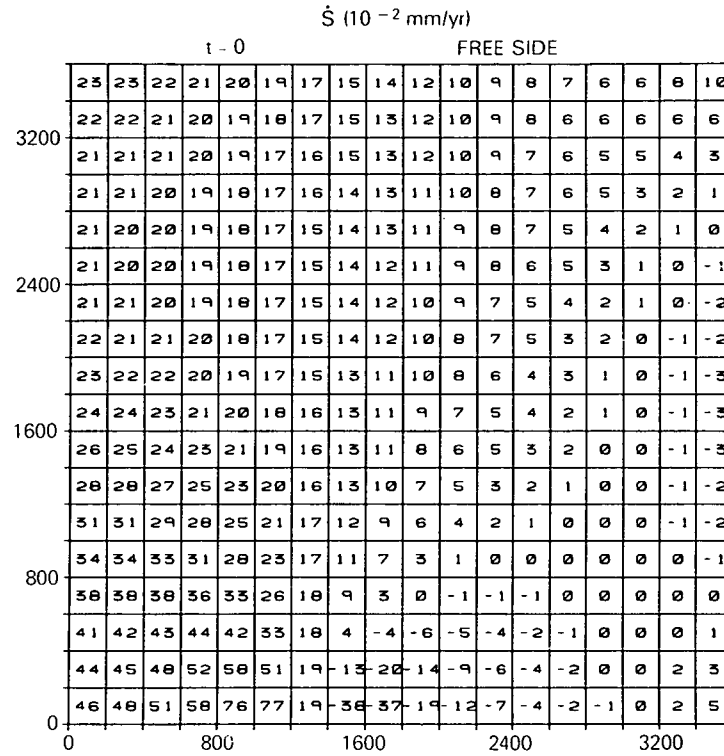
11

$\dot{S}$ (10^{-2} mm/yr)

t - 0   FREE SIDE

3200																		
23	23	22	21	20	19	17	15	14	12	10	9	8	7	6	6	8	10
22	22	21	20	19	18	17	15	13	12	10	9	8	6	6	6	6	6
21	21	21	20	19	17	16	15	13	12	10	9	7	6	5	5	4	3
21	21	20	19	18	17	16	14	13	11	10	8	7	6	5	3	2	1
21	20	20	19	18	17	15	14	13	11	9	8	7	5	4	2	1	0
21	20	20	19	18	17	15	14	12	11	9	8	6	5	3	1	0	-1
21	21	20	19	18	17	15	14	12	10	9	7	5	4	2	1	0	-2
22	21	21	20	18	17	15	14	12	10	8	7	5	3	2	0	-1	-2
23	22	22	20	19	17	15	13	11	10	8	6	4	3	1	0	-1	-3
24	24	23	21	20	18	16	13	11	9	7	5	4	2	1	0	-1	-3
26	25	24	23	21	19	16	13	11	8	6	5	3	2	0	0	-1	-3
28	28	27	25	23	20	16	13	10	7	5	3	2	1	0	0	-1	-2
31	31	29	28	25	21	17	12	9	6	4	2	1	0	0	0	-1	-2
34	34	33	31	28	23	17	11	7	3	1	0	0	0	0	0	0	-1
38	38	38	36	33	26	18	9	3	0	-1	-1	-1	0	0	0	0	0
41	42	43	44	42	33	18	4	-4	-6	-5	-4	-2	-1	0	0	0	1
44	45	48	52	58	51	19	-13	-20	-14	-9	-6	-4	-2	0	0	2	3
46	48	51	58	76	77	19	-36	-37	-19	-12	-7	-4	-2	-1	0	2	5

0   800   1600   2400   3200

(Y-axis labels: 3200, 2400, 1600, 800, 0)

Figure 5: Rates of crustal thickening at t=0+ for the same simulation as in Figure 3. The element rates are obtained by averaging the four nodal values for each element.

punch. Concerning this latter observation we find that although gravity is acting on the topography to reduce the rate of uplift at the corner of the punch, this effect is not large. The extreme distortion of the elements around the punch corner make us cautious about speculating whether this effect is real or a limitation of the finite element procedure.

The preceding discussion has emphasized crustal thickness and vertical movements. In fact, the original motivation for the punch/sheet model came from similarities between predicted and observed horizontal deformations. Figures 7 and 8 show computed values of the horizontal components of the strain rate tensor.

The analogy between some of the features observed from this model and those observed in Asia was first discussed by Molnar and Tapponier (1975; see also Tapponier, et al., 1982). Among the most important characteristics are the crustal thickening in front of the punch, the shearing and
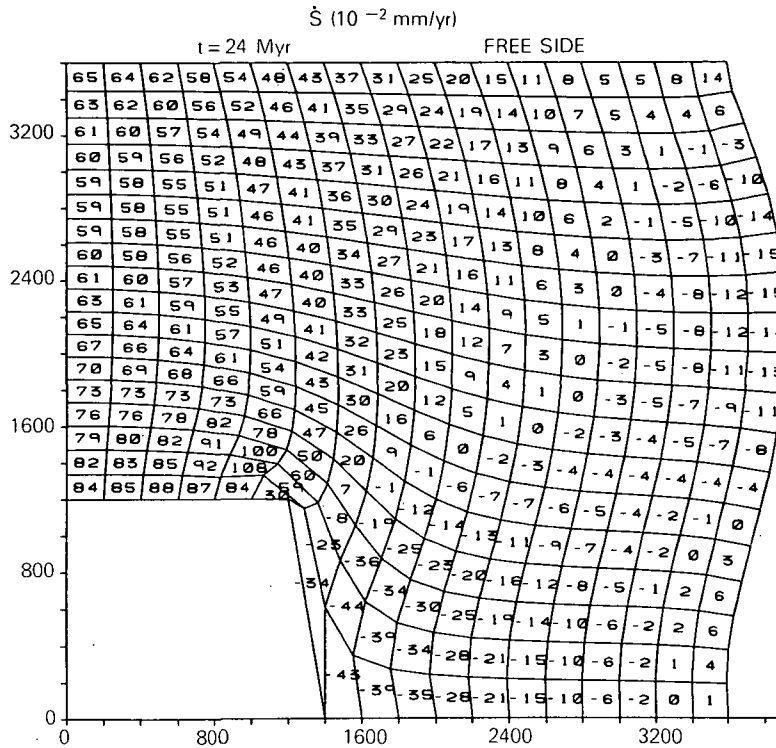
Figure 6: Same as Figure 5, but t= 24 million years.

lateral extrusion of material to the east beyond the corner of the punch, the termination of this shearing by either compression (in the case of fixed boundaries) or extension (free boundaries), and shear to the east of the punch. These phenomena are all observed to some degree in Asia, and seem to be a consequence of the collision with India.

Since north-south compression dominates the deformation in front of the punch it is interesting to take a closer look at the behavior of this quantity. The compression rate is greatest at the corner of the punch, and decreases with distance away from the punch. As shown in Figure 9, however, the compression in front of the center of the punch increases out to a distance of about 1000 km from the impact line, then decreases. The position of this extremum shows little variation with time if the origin is moved northward along with the advancing punch. A similar qualitative behavior can be deduced from the analytical expressions of Houseman, et al., but the quantitative behavior seen here is quite different. The analytical equations predict that the strain rate maximum should occur at
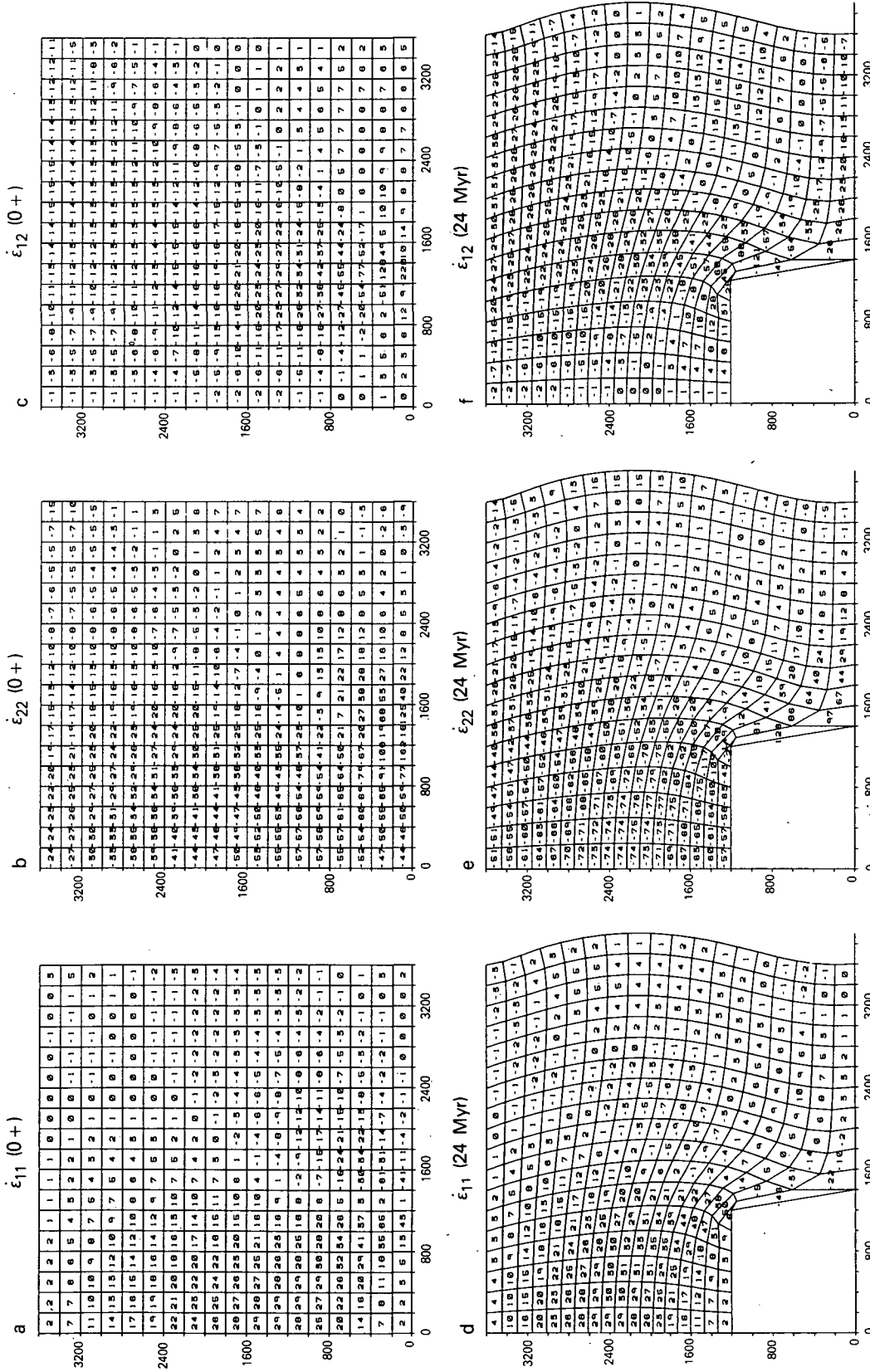
13

Figure 7: Horizontal strain rates for model with free lateral boundary.

a. east-west strain rate at t=0+.
b. north-south strain rate at t=0+.
c. shear strain rate at t=0+.

d. east-west strain rate at t=24 Myr.
e. north-south strain rate at t=24 Myr.
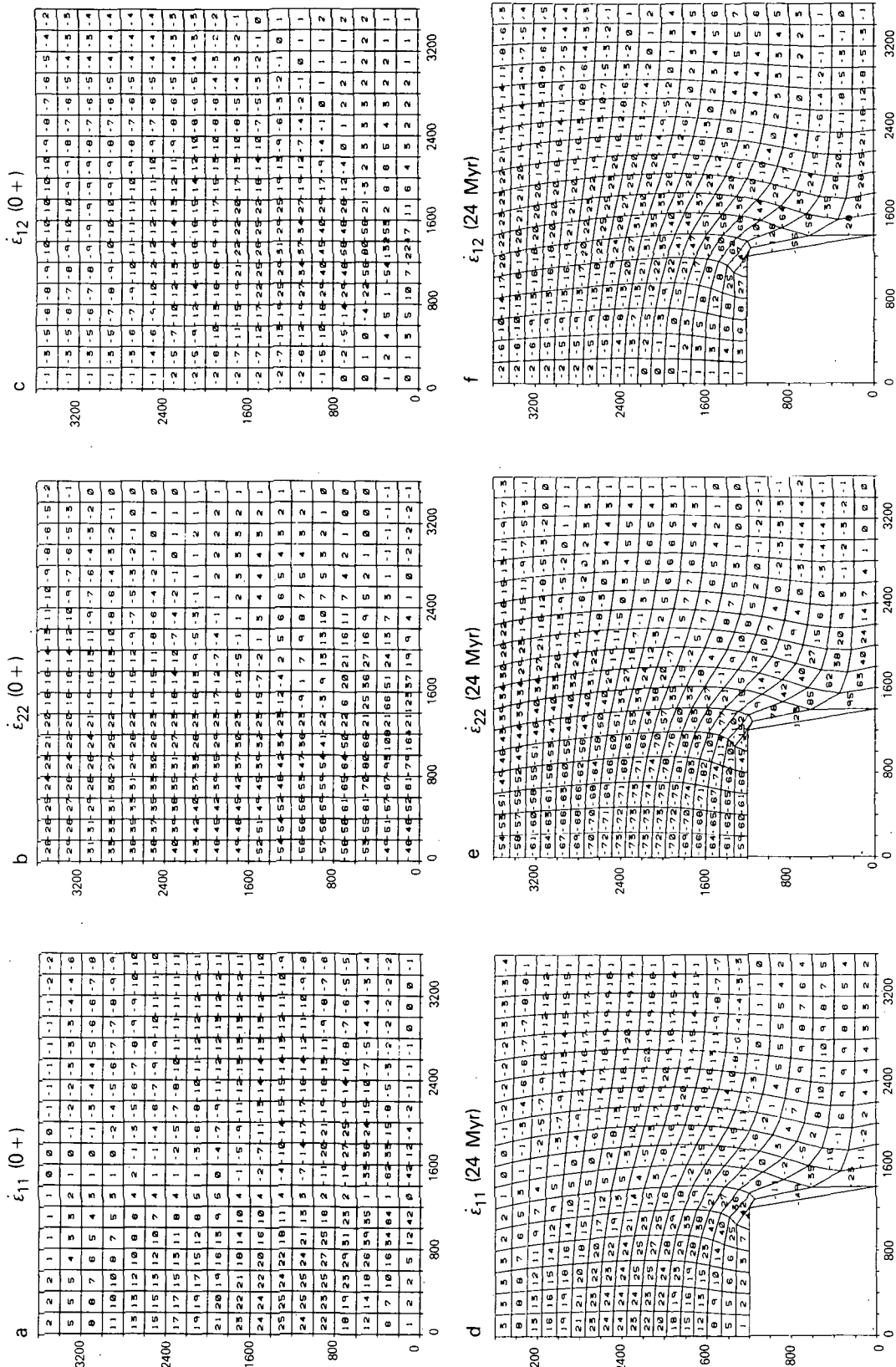f. shear strain rate at t=24 Myr.

14

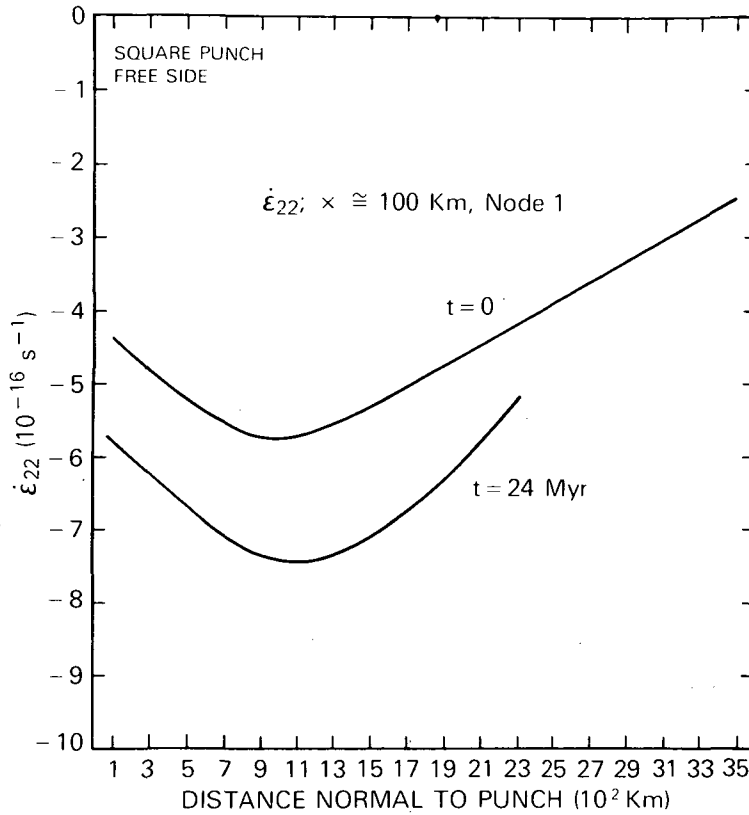Figure 8: Same as Figure 7 except for fixed lateral boundary.

15

Figure 9: North-south strain rate versus distance from the punch.

$x = $ lambda/(6 pi) where lambda is the wavelength of the (sinusoidal approximation to the) punch.

Choosing lamdba to be about 5000 km corresponding to the velocity dropping from its peak value to

zero over a 1/4 wavelength interval of 1250 km gives a predicted peak at 265 km from the punch.

This analytically predicted peak occurs much closer to the punch than is observed in the numerical

simulations. Apparently significant inaccuracies are introduced in the analytical calculations by the

approximations that are employed. In particular, the assumption of a sinusoidal variation in the

velocity distribution on the x axis produces a region of southward as well as northward flow. The

transverse components of stress and flow are also ignored in the analytical treatment. The near in-

variance of the location of the strain rate extremum appears to be a feature of a linear rheology.

Preliminary calculations using a power law rheology with $n = 3$ indicate that the extremum migrates

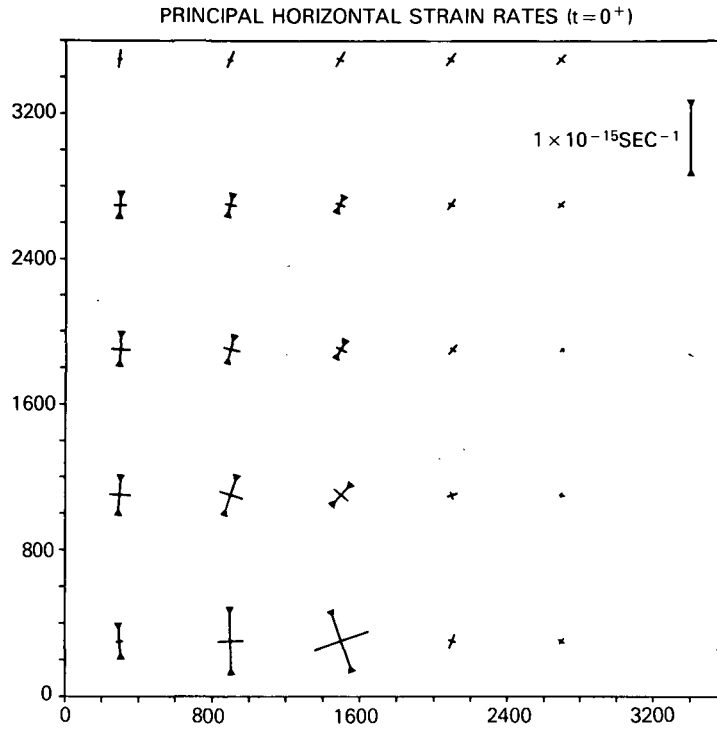away from the punch much more rapidly in the nonlinear case. A related modeling result by Melosh

Figure 10: Principal strain rates at t=0+ for free lateral boundary problem.

(1976) shows that postseismic stress propagates more rapidly into the interior of a layered nonlinear (as opposed to linear) viscoelastic earth.

An example of the principal strain rates that are deduced from the model are shown in Figure 10. The modes of deformation in different locales can be classified by applying a generalization of the Anderson brittle failure criteria to the viscous flow occurring here. Accordingly a compressive (thrusting) regime dominates where the vertical strain rate is the largest of the principle strain rates, a shearing regime exists when the vertical strain rate is the intermediate value of the three principal values, and an extensional (normal) regime dominates when the vertical strain is the least of the principle values. The classification is shown for two different times in Figure 11. The portion of the sheet dominated by compression increases with time and the shearing zones decrease in areal extent. In particular, the zone of left lateral shearing occurring to the immediate northwest of the punch is displaced northward as the punch progresses into the sheet. Of course, the classification of different
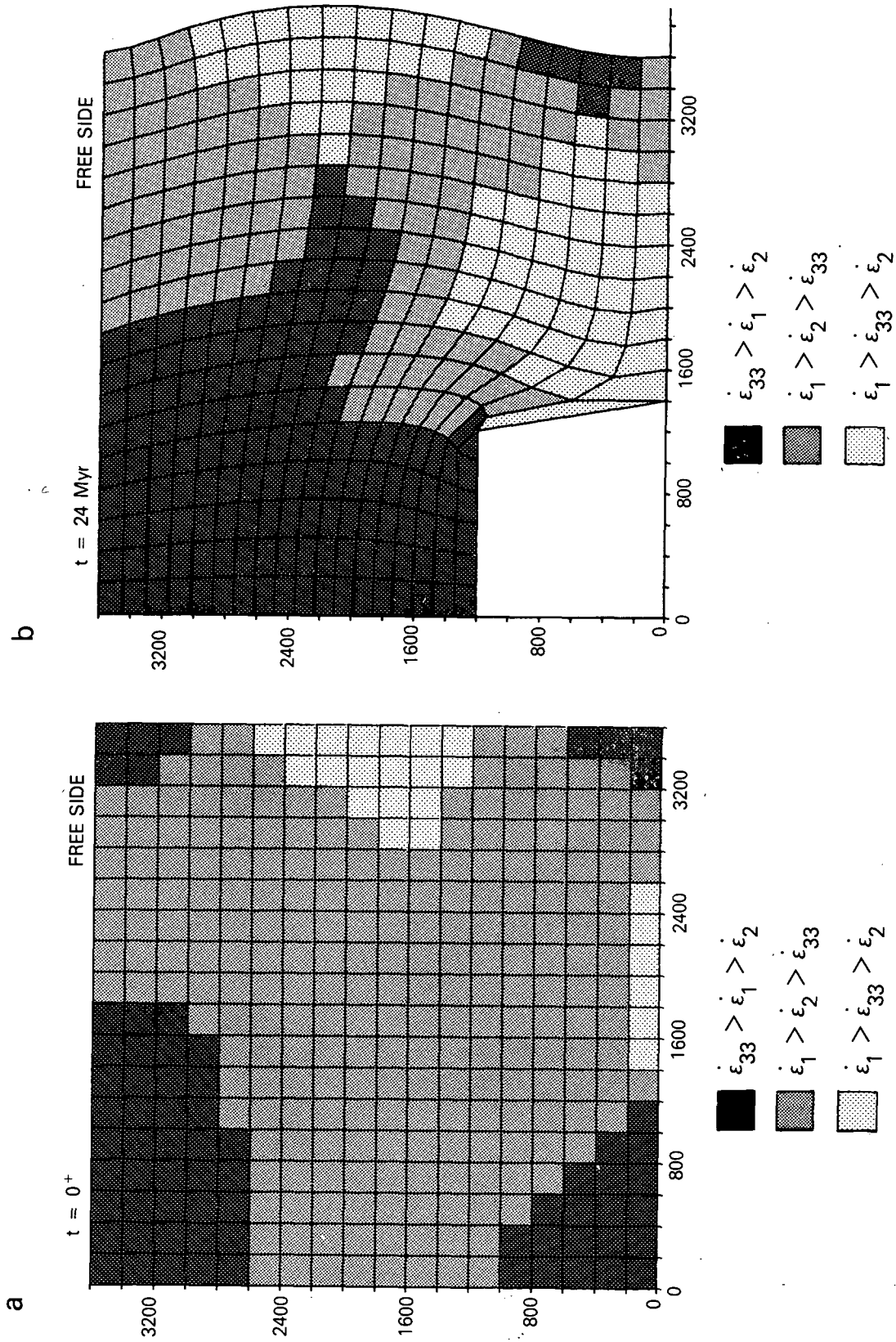
17

Figure 11: Strain rate regimes classified according to dominant deformation mechanism. Free lateral boundary.
a. t=0+.
b. t=24 Myr.

18

regions is strongly influenced by boundary conditions. Not only is the extensional behavior on the right side dependent on the stress free boundary conditions there, but also it would be reasonable to expect that shearing would be more important near the northern boundary if roller-type boundary conditions permitting eastward sliding were imposed.

Another integrated quantity which naturally emerges from the numerical calculations is the change in the areal extent of the elements adopted for the finite element grid. For the problem with a free lateral boundary, areal contraction occurs to the north and east of the punch whereas areal expansion occurs to the southwest and extreme east as shown in Figure 12. For the problem with a fixed lateral boundary, the region of contraction is larger (contraction occurs at the lateral boundaries) and that of expansion, smaller.

The preceding discussion has focused attention on the general behavior of the punch/viscous sheet model and compared results using different boundary conditions. Although an examination of all reasonable variations in model parameters would require considerably more space than can be allotted to this paper, some insight into the sensitivity of model results to parameter variations can be presented here. Viscosity, crustal densities, and lithospheric thickness enter the calculations through the right hand side of equations 3, 4, 8 and 9. In most of our calculations with a linear rheology we have found that this term has little importance. In fact most of the observed horizontal deformation patterns remain substantially unaltered if the crustal and mantle densities are set equal. For the densities shown in Table I, the gravitational term tends to be small for B values (= two times viscosity) greater than about 1×10^{23} Pa. sec unless the lithosphere is very thin or gradients in crustal thickness are very large. For example, the grid distortions and crustal thicknesses for B = 1×10^{22} Pa. sec are shown in Figure 13. The reduced crustal thicknesses are due to the inability of the sheet to maintain significant vertical straining against gravitationally induced stresses.

The distribution of velocities on the punch has a profound effect on the results. Although this statement is intuitively obvious, it has considerable importance for comparisons between the present
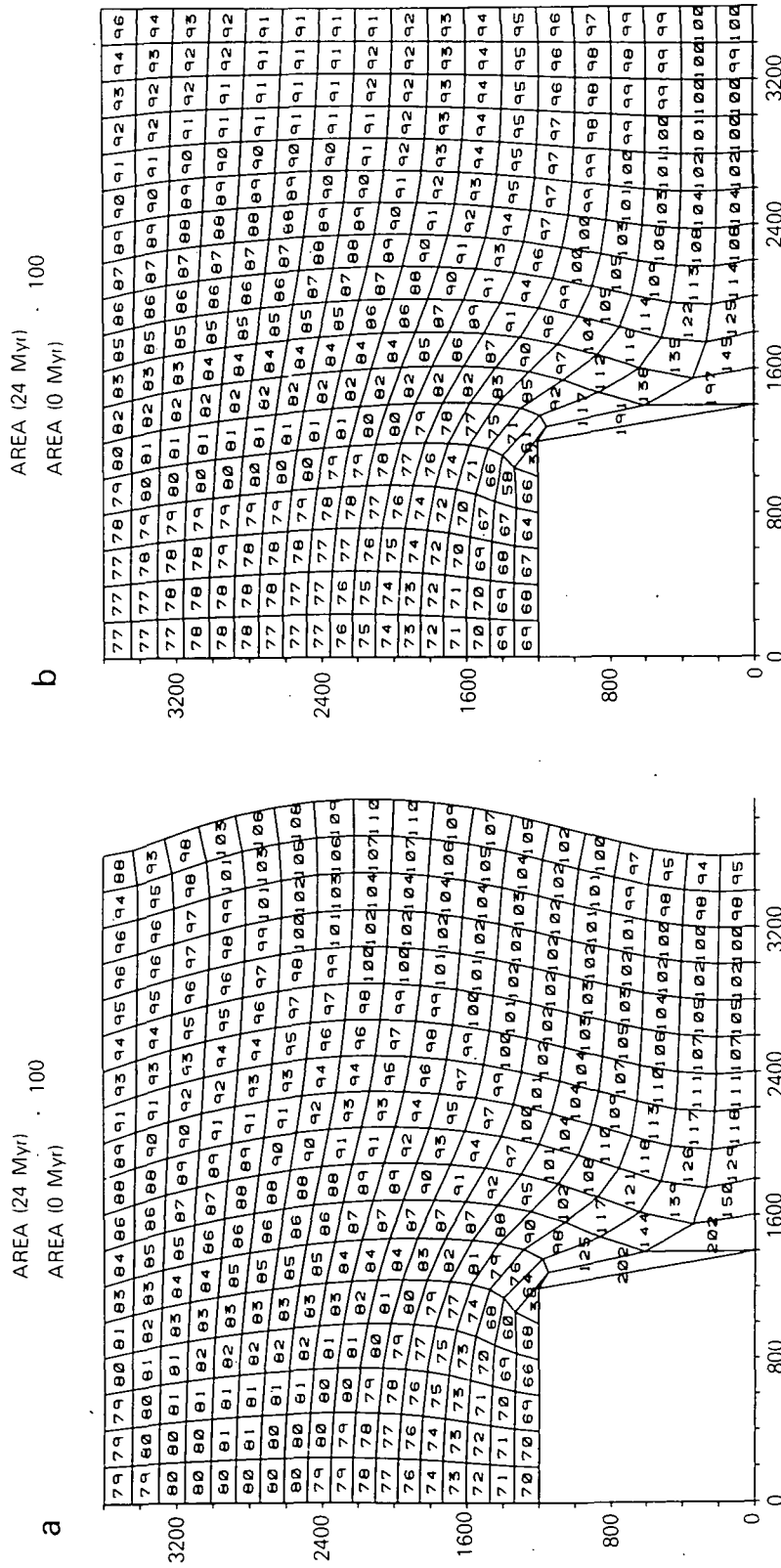
19

$$\frac{\text{AREA (24 Myr)}}{\text{AREA (0 Myr)}} \cdot 100$$

a

$$\frac{\text{AREA (24 Myr)}}{\text{AREA (0 Myr)}} \cdot 100$$

b

Figure 12: Ratio of element areas at t=24 Myr to those at t=0.
a. free lateral boundary.
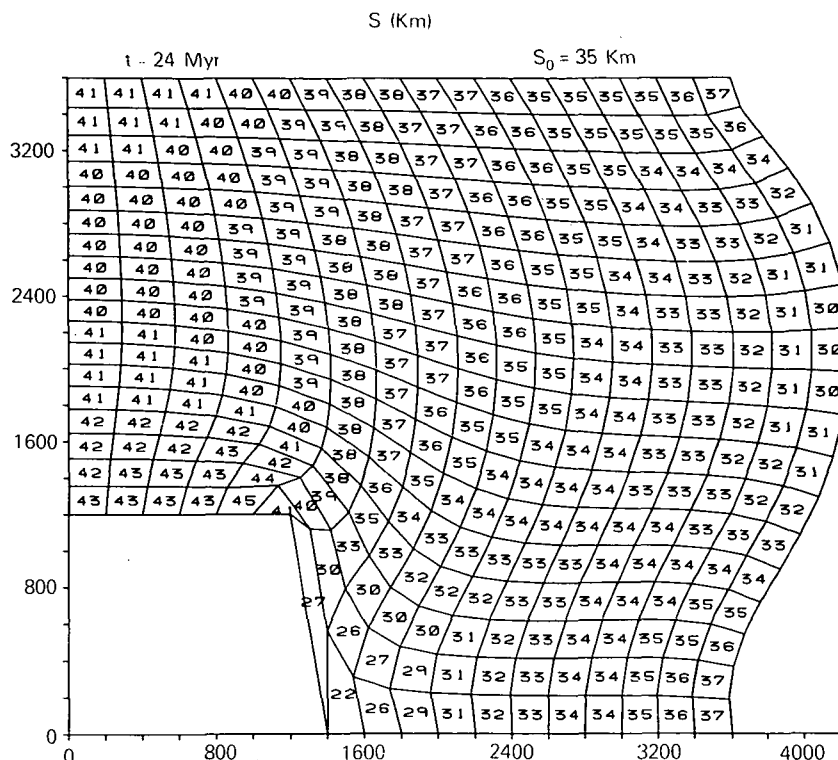b. fixed lateral boundary.

Figure 13: Low viscosity result analagous to Figure 3. $B = 1 \times 10^{22}$ Pa. sec, or 1/100th that of the earlier results.

calculations with the earlier finite difference work of England and McKenzie (1982, 1983). In the earlier work, the punch could not be represented by a moving boundary, so a flux boundary condition was imposed on the bottom boundary of the grid. The calculations were performed on a fixed grid in an Eulerian frame of reference. As a consequence the grid of nodal points was fixed in space rather than moving with the deformation. The flux boundary conditions was a flow of material at a velocity of 50 mm/yr northward between the boundary center and a point half-way across the punch. The velocity distribution then decreased to zero at the punch edge via a cosine squared law. In the early stages of the collisions, the vertical straining, compression, and crustal thickening are concentrated at the edge of the punch. The observed features are qualitatively similar to those seen with the finite element, moving boundary calculations except, of course for the deformation observed south of the boundary in the flux calculations. As time advances, a punch boundary can be defined by calculating the position of material that was initially on the grid boundary when the collision began.

21

When this is done, as in Figure 14, one finds that the punch becomes progressively more sheared as it deforms according to the same rheological law as the sheet. This deformation includes a rounding of the velocity distribution. The center of the boundary becomes the leading point and the sharp corner at the punch edge is eliminated. As a consequence crustal thicknesses become concentrated near the middle of the leading edge of the advancing material. The pattern of horizontal straining is also altered to some degree. These results suggest several important features about the deformation. The concentration of the most intense deformation about the punch corner requires the maintenance of a sharp corner throughout the duration of the collision. If the punch is to represent the continental portion of a tectonic plate, then the continental material must remain fairly rigid and unsheared. If,
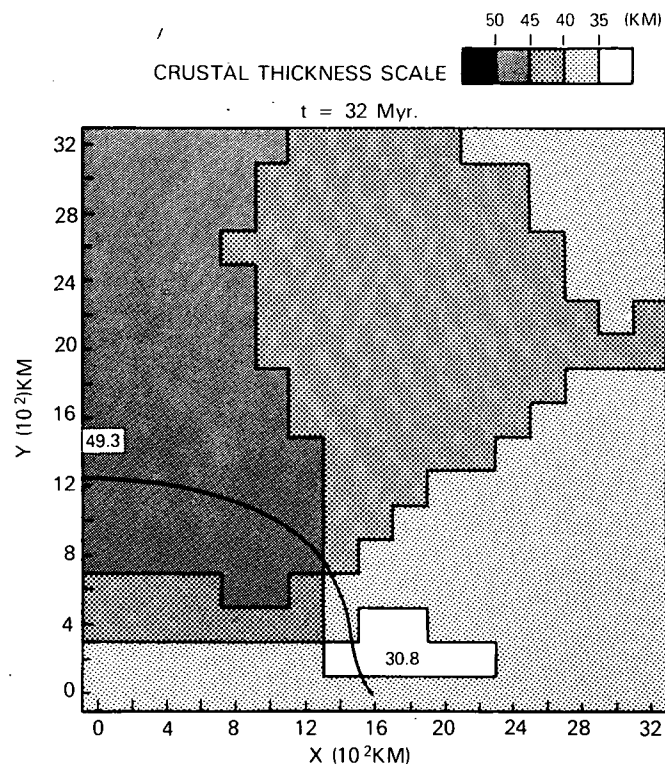

Figure 14: Crustal thicknesses and punch boundary obtained from flux boundary condition problem, t=32 Myr. A flow northward of 50 mm/yr occurs between X=0 and X=800 km; the velocity then decreases to 0 at X=1600 km according to a cosine squared law. The finite element grid is fixed and a Eulerian analysis is used. The solid line shows the position of material that was on the southern grid boundary at t=0. This punch boundary has progressively sheared both due to the velocity distribution and the non-rigid character of the punch. Crustal thickness has a maximum at X=0.

22

however, the continental ram does undergo significant shear, then the deformation within the sheet becomes concentrated in front of the leading point of the punch.

SUMMARY

Our modeling efforts are based almost exclusively on the geophysical and mathematical foundation provided by the work of England, McKenzie, Houseman, and Sonder. Therefore, some of the results presented here for the fixed lateral boundary conditions will qualitatively agree with the finite element results of these workers. The new features introduced here include a free lateral boundary, a rigid punch (as opposed to a tapered and sheared punch used in earlier work), and a more detailed analysis of several aspects of the model. Particularly important features found in our calculations are the sensitivity of compression to position from the punch, the relative absence of strain propagation away from the punch for a linear viscous flow (as opposed to the propagation with a power law flow), the termination of shearing by compression or extension depending on boundary conditions, and the effect of punch rigidity on deformation near the corners and the center of the punch. New results have been presented on crustal thickening rates (which approach 1 mm/yr for the parameters used herein), changes in the area of the mass elements, and the classification of deformation regimes.

REFERENCES

Bird, P., M. N. Toksoz, and N. H. Sleep, "Thermal and mechanical models of continent-continent convergence zones," *J. Geophys. Res.*, 80, 4405-4416, 1975.

Condie, K. C., *Plate Tectonics & Crustal Evolution*, Pergamon Press, New York, 1982.

England, P., G. Houseman, L. Sonder, "Length scales for continental deformation in convergent, divergent, and strike-slip environments: analytical and approximate solutions for a thin viscous sheet model," *J. Geophys. Res.*, 90, 3351-3557, 1985.

England, P., and D. P. McKenzie, "A thin viscous sheet model for continental deformation," *Geophys. J. R. Astron. Soc.*, 70, 295-321, 1982. (Correction, *Geophys. J. R. Astron. Soc.*, 73, 523-532, 1983.)

Houseman, G. and P. England, "Finite strain calculations of continental deformation I: method and general results for convergent zones," *J. Geophys. Res.*, in press, 1985.

Melosh. H. J., "Nonlinear stress propagation in the Earth's upper mantle," *J. Geophys. Res.*, 81, 5621-5632, 1976.

Molnar, P., and P. Tapponier, "Cenozoic tectonics of Asia: effects of a continental collision," *Science*, 189, 419-426, 1975.

Oxburgh, E. R., "Flake tectonics and continental collision," *Nature*, 239, 202-204, 1972.

Tapponier, P., G. Peltzer, A. Y. Le Dain, R. Armijo, and P. Cobbold, "Propagating extrusion tectonics in Asia: New insights from simple experiments with plasticine," *Geology*, 10, 611-616, 1982.

Tapponier, P. and P. Molnar, "Active Faulting and Tectonics in China," *J. Geophys. Res.*, 82, 2905-2930, 1977.

Vilotte, J. P., M. Daignieres, and R. Madariaga, "Numerical models of intraplate deformation: simple mechanical models of continental collision," *J. Geophys. Res.*, 87, 10709-10728, 1982.

Zhao, W-L., and W. J. Morgan, "Injection of Indian crust into Tibetan lower crust: a 2-D finite element model study," *EOS, Trans. Am. Geophys. U.*, 66, 375, 1985.

BIBLIOGRAPHIC DATA SHEET

1. Report No. NASA TM 86235	2. Government Accession No.	3. Recipient's Catalog No.
4. Title and Subtitle Intraplate Deformation Due To Continental Collisions: A Numerical Study of Deformation In A Thin Viscous Sheet		5. Report Date October, 1985
		6. Performing Organization Code 621
7. Author(s) Steven C. Cohen		8. Performing Organization Report No. 86B0019
9. Performing Organization Name and Address Geodynamics Branch Laboratory for Terrestrial Physics Goddard Space Flight Center		10. Work Unit No.
		11. Contract or Grant No.
12. Sponsoring Agency Name and Address National Aeronautics Space Administration Washington, DC		13. Type of Report and Period Covered Technical Memorandum
		14. Sponsoring Agency Code

15. Supplementary Notes

16. Abstract

Continental collisions can result in the transmission of stress from the boundary between tectonic plates into the plate interiors. Extensive crustal deformations characterized by both horizontal and vertical crustal movements have occurred as a consequence of collisions in both contemporary and ancient tectonic environments. These deformations have been analyzed by a number of observers who in recent years have begun to propose various geological and numerical models of the collision processes. One of the more successful models, involves the penetration of a rigid punch (one plate) into a deformable sheet (another plate). For example, this model has been used by Tapponier and Molnar (1977), Vilotte, et al. (1982), and others as an aid in understanding the tectonics of the India-Eurasia collision. In this paper we examine in detail some of the features of this model as first formulated by England and coworkers (1982, 1983, 1985; Houseman and England, 1985). Using a linear viscous flow law for most of our calculations, we compute the magnitude and rate of change of crustal thickness, the velocity of various mass points, strain rates and their principal axes, modes of deformation, areal changes, and stress. Particular attention is payed to the role of lateral boundary conditions. In general a free lateral boundary reduces the magnitude of changes in crustal thickening (compared to a fixed lateral boundary) by allowing material to more readily escape the advancing punch. The shearing that occurs diagonally in front of the advancing punch terminates in compression or extension depending on whether the lateral boundary is fixed or free to move. When the ratio of the diameter of the punch to that of the viscous sheet exceeds about one-third, the deformation in front of the punch is insensitive to the specific choice of lateral boundary conditions. Although gravitational effects can then reduce the rate of compression and crustal thickening in a plate deforming by nonlinear viscous flow, this effect is minor for linear flow unless the viscosity is small and/or the topographic relief substantial. When the punch is rigid and maintains sharply defined edges, deformation is concentrated near the punch corners; hence gravitational stresses are first seen there. However, if the punch is not rigid the attendent shearing results in the deformation being concentrated near the leading point (center) of the punch. While many of the other observed qualitative deformation features are present for both linear and nonlinear flow laws, some change significantly. In particular, the variation in compression rate with distance from the punch is sensitive to the choice of rheological law. With a linear law, the axial distance from the middle of the punch to the point of local maximum compression is relatively invariant with time. This maximum occurs much farther from the punch than is predicted from recently published approximate analytical expressions. For a nonlinear law, the location of the maximum propagates away from the punch/sheet boundary.

17. Key Words (Selected by Author(s)) geodynamics, continental collisions, numerical models	18. Distribution Statement Unlimited Unclassified Category Listing 46		
19. Security Classif. (of this report) Unclassified	20. Security Classif. (of this page) Unclassified	21. No. of Pages	22. Price*

GSFC 25-44 (10/77)